Jarosite in a Pleistocene East African saline-alkaline paleolacustrine deposit: Implications for Mars aqueous geochemistry

Lindsay J. McHenry,[1] Vincent Chevrier,[2] and Christian Schröder[3,4]

Received 29 June 2010; revised 7 December 2010; accepted 23 December 2010; published 6 April 2011.

[1] Jarosite occurs within altered tephra from the saline-alkaline paleolake deposits of Pliocene-Pleistocene Olduvai Gorge, Tanzania. Zeolites (mainly phillipsite), authigenic K-feldspar, and Mg/Fe-smectites dominate the mineral assemblage, indicating saline-alkaline diagenetic conditions (pH > 9). As jarosite is ordinarily an indicator of acidic conditions on Earth and Mars, its association with such undisputed high-pH indicators is unexpected. Of 55 altered tephra samples collected from the paleolake basin and margin deposits, eleven contained jarosite detectable by X-ray Diffraction (XRD) (>0.15%). Mössbauer spectroscopy, Fourier Transform Infrared Reflectance (FTIR), Electron Probe Microanalysis (EPMA), X-ray Fluorescence (XRF), and Scanning Electron Microscopy (SEM) analyses confirm the presence and nature of the jarosite. This paper documents this occurrence and presents mechanisms that could produce this unusual and contradictory mineral assemblage. We favor a mechanism by which jarosite formed recently, perhaps as modern ground and meteoric water interacted with and oxidized paleolacustrine pyrite, providing local and temporary acidic conditions. However, local groundwater (at modern springs) has a pH > 9. In recent studies of Mars, the presence of jarosite or other Fe or Mg sulfates is often used to indicate dominantly acidic conditions. Regardless, the current study shows that jarosite can form in sediments dominated by alkaline minerals and solutions. Its coexistence with Mg/Fe smectites in particular makes it relevant to recent observations of Martian paleolakes.

Citation: McHenry, L. J., V. Chevrier, and C. Schröder (2011), Jarosite in a Pleistocene East African saline-alkaline paleolacustrine deposit: Implications for Mars aqueous geochemistry, *J. Geophys. Res.*, *116*, E04002, doi:10.1029/2010JE003680
.

1. Introduction

1.1. Jarosite on Mars and Earth

[2] On Earth and on Mars, the presence of the hydrous iron sulfate mineral jarosite ($(K, Na, H_3O)Fe^{3+}_3(OH)_6(SO_4)_2$) most often indicates aqueous, acidic, and oxidizing conditions [e.g., *Stoffregen et al.*, 2000; *Elwood Madden et al.*, 2004; *Papike et al.*, 2006]. Jarosite typically indicates water-limited rock alteration [*Elwood Madden et al.*, 2004] and thus evaporation in acidic environments [e.g., *Tosca et al.*, 2005], acid-sulfate alteration of basalt under solfatara [e.g., *Bishop et al.*, 2007] or hydrothermal [e.g., *Morris et al.*, 1996] conditions or weathering of sulfide-rich deposits in oxidative environments [e.g., *Burns and Fisher*, 1990; *Chevrier et al.*, 2004, 2006; *Fernández-Remolar et al.*, 2005]. It is rarely observed under conditions of pH > 4, and typically forms at lower pH [e.g., *Dutrizac and Jambor*, 2000; *Stoffregen et al.*, 2000]. While some life forms on Earth have adapted to acidic conditions, *Knoll et al.* [2005] argue that such conditions would have posed a challenge to prebiotic reactions that are thought to have played a role in the origin of life.

[3] The Mars Exploration Rover (MER) Opportunity detected the presence of jarosite on Mars [*Klingelhöfer et al.*, 2004]. *Burns* [1986] had long predicted that jarosite or other Fe^{3+} sulfate minerals would be present in the Martian regolith. Recent data from orbiters have revealed that the layered sulfate deposits of Meridiani Planum are extensive, and that similar deposits are abundant elsewhere on Mars [e.g., *Bibring et al.*, 2007]. Data from Opportunity allow for a detailed analysis of the mineralogical and geochemical context of one occurrence of Martian jarosite. Despite the abundance of jarosite at the Opportunity site (it accounts for 29% of the Fe present in Burns Formation outcrop rocks [*Morris et al.*, 2006b]) it has not yet been detected at this site from orbit [*Murchie et al.*, 2009]. The first orbital detection

[1]Department of Geosciences, University of Wisconsin-Milwaukee, Milwaukee, Wisconsin, USA.
[2]W. M. Keck Laboratory for Space and Planetary Simulation, Arkansas Center for Space and Planetary Sciences, University of Arkansas, Fayetteville, Arkansas, USA.
[3]Department of Hydrology, University of Bayreuth, Bayreuth, Germany.
[4]Center for Applied Geoscience, Eberhard Karls Universität, Tuebingen, Germany.

0148-0227/11/2010JE003680

of jarosite on Mars was near Ius/Melas Chasma in the Valles Marineris region [*Milliken et al.*, 2008], and it has since also been identified in the potential paleolake deposits of Columbus Crater at Terra Sirenum [*R. Wray et al.*, 2009] and within the vicinity of Mawrth Vallis [*Farrand et al.*, 2009]. Jarosite occurs in association with phyllosilicates, which typically form under neutral/high pH conditions, in Ius Chasma [*Roach et al.*, 2010] and in paleolake deposits [*R. Wray et al.*, 2009; *Farrand et al.*, 2009], attesting to variable pH conditions. To form and preserve abundant jarosite following the conventional model, conditions must remain acidic or water-limited over time. This is difficult in an environment dominated by basaltic weathering, as this leads to alkaline conditions by neutralizing acidity. One possible source of acidity is the oxidation of Fe^{2+} from the original igneous minerals to Fe^{3+} [*Klingelhöfer et al.*, 2004; *Morris et al.*, 2006b; *Tosca et al.*, 2008].

[4] The jarosite observed at Meridiani and elsewhere today could also be a more recent (perhaps even Amazonian) phenomenon compared to the original late Noachian/early Hesperian time of deposition [e.g., *Fairén et al.*, 2009]. Jarosite, especially in its pulverulent (poorly crystalline) form, is sensitive to changes in pH, temperature, oxidation conditions, and water abundance and therefore might not have been able to withstand the pre-Amazonian environmental changes. If true, jarosite may have formed much later, under more favorable climatic conditions (within the last 2 Ga), as earlier formed rocks and sediments interacted with small volumes of acidic brines [*Fairén et al.*, 2009]. Under these conditions, jarosite needs not have formed as part of an equilibrium assemblage with the other minerals observed, and could reflect different diagenetic conditions. Regardless of when it was formed, the rate at which jarosite dissolves in contact with aqueous fluids limits the amount of time a jarosite-bearing deposit could have been exposed to such conditions since formation [e.g., *Elwood Madden et al.*, 2009]. *Elwood Madden et al.*'s [2009] experiments suggest that, depending on the temperature and fluid composition, a 10 μm particle of jarosite can last from 1.5 years (in warm, dilute water) to 1 Ma (in cold, NaCl brines). Concretionary jarosite is more resistant to weathering; Miocene-aged concretionary jarosite has been observed in the Rio Tinto area of Spain [*Fairén et al.*, 2009].

[5] Another hypothesis suggests that Martian jarosite formed as a result of the interaction of dust and sulfate aerosols within a large ice deposit, possibly formed at a time of high obliquity [*Niles and Michalski*, 2009]. This model would allow locally acidic conditions to persist without being neutralized by interaction with the basaltic regolith, and could allow for localized pockets of acidic alteration over a regional scale.

[6] The presence of zeolites in certain Martian environments is often considered unlikely because of the alkaline conditions they tend to form in, in contrast to the acidic conditions implied by the Mg and Fe sulfates identified [e.g., *Clark et al.*, 2005; *Ming et al.*, 2006]. However, *Ruff* [2004] found spectral evidence in support of a zeolite component to Martian dust, and analcime ($NaAlSi_2O_6 \cdot H_2O$), a zeolite mineral typical of saline-alkaline environments [*Langella et al.*, 2001], has now been identified at Nili Fossae on Mars [*Ehlmann et al.*, 2009]. The abundance and frequency of zeolites on Mars is difficult to assess, in part because of the inability to distinguish between certain zeolites and polyhydrated sulfates in spectral data from the Compact Reconnaissance Imaging Spectrometer for Mars (CRISM) on the Mars Reconnaissance Orbiter (MRO) [e.g., *J. J. Wray et al.*, 2009].

[7] A growing number of mineralogically complex and in some cases nonacidic occurrences of jarosite on Earth show that jarosite is not an indicator of a single diagenetic environment. For example, *Ashley et al.* [2004] found jarosite formed from oxidizing pyrite in a neutral freshwater spring environment in Loboi Swamp, Kenya. *Leveille* [2007] found jarosite formed in acidic microenvironments in otherwise highly buffered carbonate sediments in a polar desert. *Darmody et al.* [2007] found jarosite forming (from pyrite weathering) in a cold, arid, and carbonate buffered environment in Swedish Lapland. *Benison and LaClair* [2003] first suggested the relevance of Western Australian saline lakes as Mars analogs. *Gray* [2001] and *Baldridge et al.* [2009] describe jarosite in these laterally variable phyllosilicate-bearing lacustrine environments, where pH and oxidation conditions vary both horizontally and vertically on a scale of meters to tens of meters, allowing the coexistence of neutral and acidic mineral assemblages in a small area.

[8] Jarosite is also found in altered tephra in the saline-alkaline Pliocene-Pleistocene paleolake deposits of Olduvai Gorge, Tanzania [*Hay*, 1973; *McHenry*, 2009]. At Olduvai, zeolites (mainly phillipsite, $(Ca, Na_2, K_2)_3Al_6Si_{10}O_{32} \cdot 12H_2O$), authigenic K-feldspar ($KAlSi_3O_8$), and Fe/Mg smectite dominate the mineral assemblage, indicating saline-alkaline diagenetic conditions. Phillipsite forms in altered volcanic ashes in closed basin environments only once the pH reaches 9–10 [*Langella et al.*, 2001]. A detailed review of the authigenic minerals (including bulk composition) is presented by *McHenry* [2009, 2010]. All minerals in the altered Tuff IF samples are most likely authigenic or primary volcanic, since the samples come from the interior layers of a volcaniclastic surge and air fall deposit [*Stollhofen et al.*, 2008]. The complete lack of quartz in the samples from the paleolake also limits the possibility of detrital input, as quartz is a major constituent of the detrital influx into the paleolake from the west. No glass was preserved within the paleolake deposit, but tephra can be correlated (using phenocryst composition) between paleolake center and glass-bearing paleolake margin and paleo-freshwater wetlands samples, providing access to prealteration tephra composition [*McHenry*, 2005]. Despite the abundance of zeolites and other indicators of saline-alkaline conditions (e.g., casts after trona, $Na_3H(CO_3)_2 \cdot 2H_2O$), jarosite is present within the altered tephra at some sites [*Hay*, 1973; *McHenry*, 2009].

1.2. Objectives

[9] The objectives of this study are to (1) document and constrain this unusual occurrence of jarosite in saline-alkaline paleolacustrine sediments at Olduvai, (2) develop a model that can explain this assemblage, and (3) compare this assemblage and model to data and interpretations from missions to Mars. Where possible, this study will employ techniques recently applied to the Martian surface (e.g., Mössbauer, NIR spectroscopy) for more direct comparison, and will compare the results of these methods to the results of other methods (X-ray Diffraction (XRD), Electron Probe

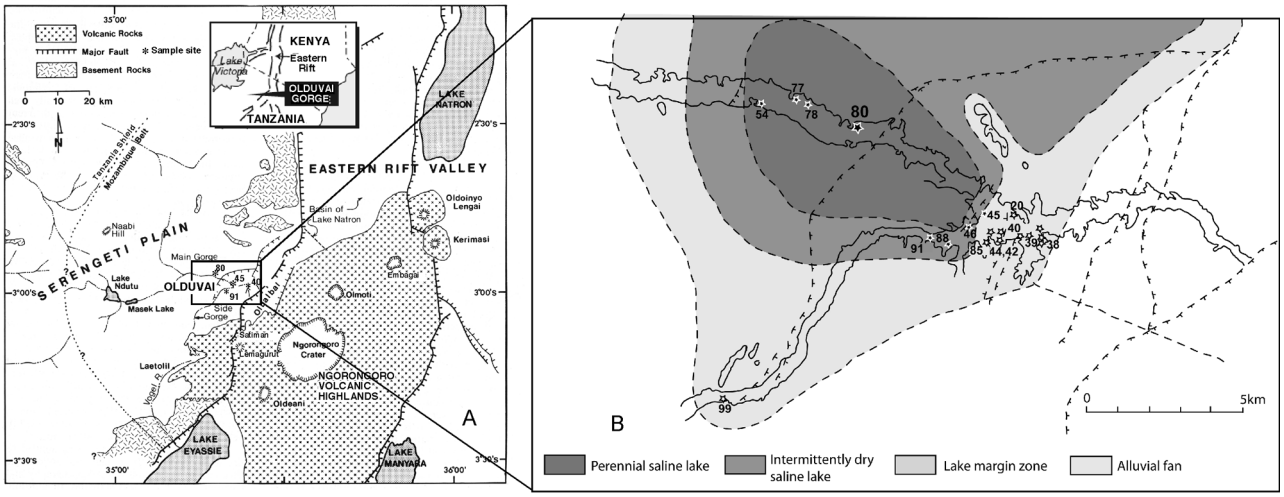

Figure 1. Maps showing location of Olduvai Gorge and sampled sites. (a) Location of Olduvai Gorge and nearby Ngorongoro Volcanic Highlands volcanic sources. (b) Map of sampled localities and Lower Bed II depositional environments. Maps after *Hay* [1976]. Copyright 1976 by the Regents of the University of California.

Microanalysis (EPMA), Scanning Electron Microscopy (SEM)) to test the consistency of the different methods.

2. Background: The Geology of Olduvai Gorge

[10] Olduvai Gorge exposes a Pliocene-Pleistocene lacustrine basin on the shoulder of the East African Rift in northern Tanzania (Figure 1). This basin is adjacent to the Ngorongoro Volcanic Highlands, which supplied the volcanic ash and sediments that make up much of the Olduvai sedimentary record. Deposition in the Olduvai basin began around 2.03 Ma [*Walter et al.*, 1992].

[11] The ~100 m thick Olduvai Formation is divided into a series of beds, including Beds I-IV, Masek, Ndutu, and Naisiusiu, from oldest to youngest. A shallow, saline-alkaline lake occupied the center of the basin during the deposition of Beds I and II, between about 1.9 and 1.7 Ma [*Hay*, 1976; *Walter et al.*, 1992]. It expanded and contracted over time in response to changes in climate, faulting, and volcanic input (Figure 1b). The presence of abundant zeolites and authigenic K-feldspar, along with casts after trona [*Hay*, 1976], indicates prolonged periods of saline-alkaline conditions in the closed-basin lake and in pores within the sediments beneath it [*McHenry*, 2010]. This paleolake can thus be considered both a depositional and a diagenetic environment.

[12] During the deposition of Bed I, a series of trachytic, trachyandesitic, and phonolitic tephra were deposited, altered, and preserved in the lake sediments. The major tephra from the lake deposit include Tuffs IA, IB, ID, IE, Ng'eju, and IF [*Hay*, 1976; *McHenry*, 2005].

3. Methods

3.1. Site Selection and Sampling

[13] Samples were initially collected in 1999, 2002, and 2006 as part of a tephra alteration and correlation project [*McHenry*, 2005, 2009, 2011; *McHenry et al.*, 2008]. The discovery of jarosite prompted more detailed sampling in 2007, 2008, and 2009 to narrow down its occurrence. Using *Hay*'s [1976] maps and facies interpretations and *McHenry*'s [2009, 2010] prior authigenic mineral results, sample sites were selected from different depositional and diagenetic environments across the paleolake deposit. Sites within the central paleolake basin, intermittently dry paleolacustrine zone, proximal and distal paleolake margin, and freshwater wetland paleoenvironments were selected and sampled (Figure 1). Sampling focused on Tuff IF because this tephra layer is thicker and more easily recognizable than the other Olduvai tephra [*McHenry*, 2005; *McHenry et al.*, 2008], and because jarosite was first recognized in it [*McHenry*, 2009].

[14] Four central paleolake basin sites (Localities 80, 54, 77, and 78) were sampled to determine the distribution of jarosite within the paleolake deposit. At Localities 80 and 54, all Bed I tephra layers were sampled to see how the presence of jarosite varied with stratigraphic position and with starting tephra composition. At Localities 80, 77, and 78, 2–6 samples per site were collected from the different layers within Tuff IF to determine the distribution of jarosite within individual exposures. At Locality 80, Tuff IF was sampled in detail (2–6 samples per site) at three sections within ~100 m of each other, to see if the jarosite occurrence is laterally consistent. One specific part of a single layer of Tuff IF at Locality 80 was initially sampled in 2006 and then resampled in 2008 and 2009. A photograph of the main Locality 80 exposure, including sample positions, is provided in Figure 2. All samples were collected in July or August, during Tanzania's dry season. About 200 g per sample were collected. Mineral precipitates were also sampled at a modern spring at Locality 78 (within meters of the sampled tephra) to help constrain the composition of modern groundwater in the area. The water from two springs at Locality 78 was also analyzed for pH and conductivity in the field.

[15] Samples of Tuff IF from three sites (Localities 91, 88, and 46b) in *Hay*'s [1976] intermittently dry lacustrine facies, five sites in the proximal paleolake margin area (Localities

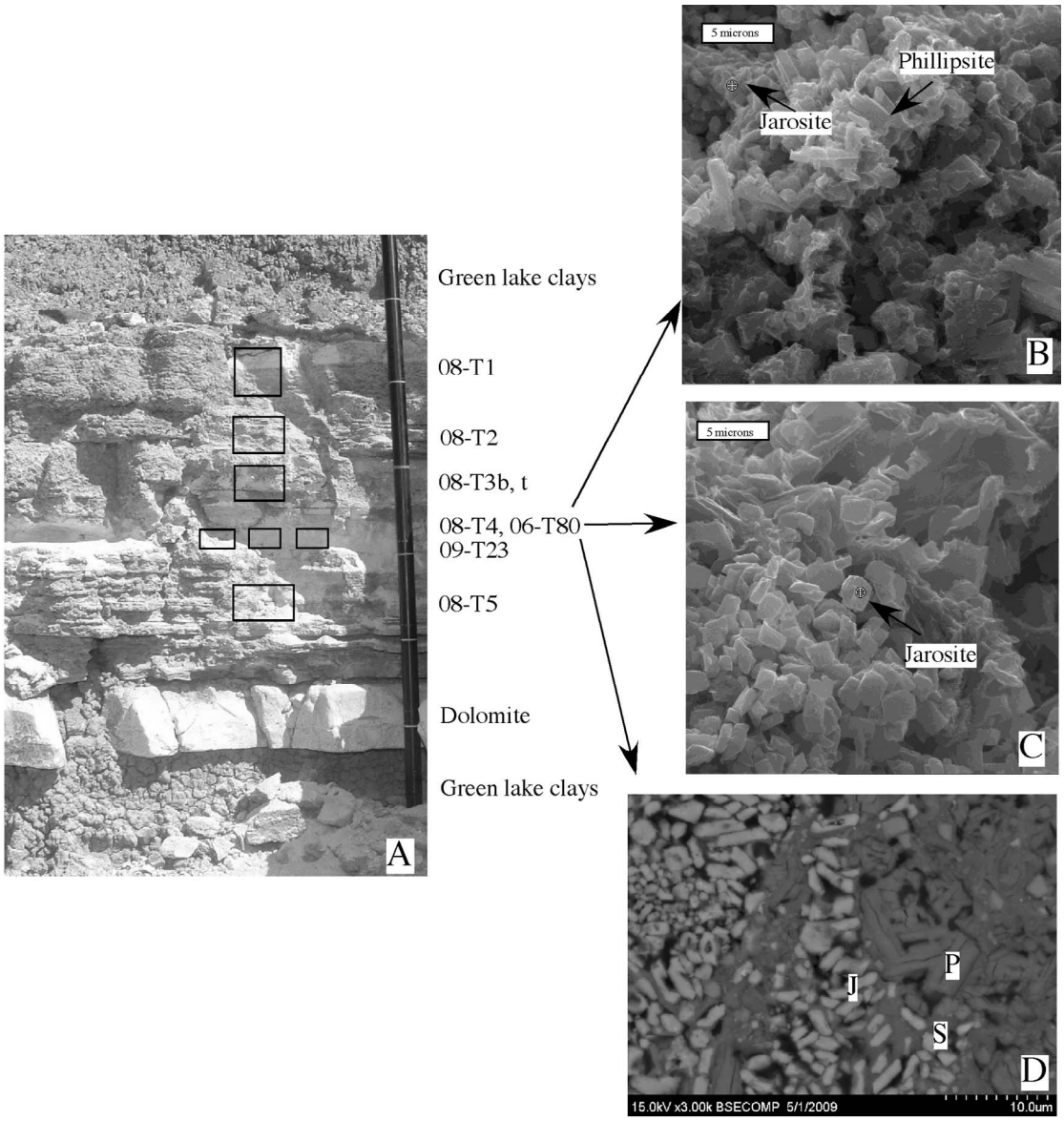

Figure 2. (a) Photograph of Tuff IF at Locality 80, with sample positions labeled. Surrounding the tuff are green, lacustrine claystones. Jarosite-bearing samples 06-T80, 08-T4, and 09-T23 were collected from a light-colored, fine-grained, powdery layer enclosed by layers of coarser, more resistant non-jarosite-bearing tephra above and below. Other paleolake basin Tuff IF sites (Localities 80E, 80W, 77, and 78) have similar layering. (b) Secondary electron (SE) SEM image of unpolished sample 06-T80, showing texturally associated jarosite and phillipsite, identified using crystal shape, qualitative EDS, and comparison to XRD results. (c) SE SEM image of a mass of small, well-defined jarosite crystals in unpolished sample 06-T80. (d) Backscattered electron (BSE) SEM image of associated jarosite (J), smectite (S), and phillipsite (P) in a polished thin section of sample 06-T80.

45, 20, 44, 42, and 85), one from the distal paleolake margin (Locality 38), and three sites within the paleo-freshwater wetlands deposit (Localities 39, 40, and 41) were also collected. Tuff IF at Locality 38 (distal paleolake margin) varied laterally in appearance and was thus sampled from multiple exposures. Together these sites represent a transect across the saline-alkaline paleolacustrine deposit, providing samples from the different bands of authigenic minerals. Table 1 lists all samples collected, with their localities, depositional/diagenetic environments, and authigenic mineral assemblages.

3.2. Sample Preparation and X-Ray Diffraction

[16] Samples were cleaned, removing any crack fillings or roots, and then crushed and finely powdered in an agate mortar and pestle. The fine powders were then mounted for random powder XRD analysis, and analyzed using a Bruker D8 Focus. Every sample was analyzed using a "quick" routine: 2–60° 2θ, 1 s/step, step size 0.02° (Cu Kα radiation, Sol-X energy dispersive detector). Samples were compared against the ICDD PDF library using Bruker's EVA software and if potential jarosite peaks were present, the sample was

Table 1. Diagenetic Environments and Authigenic Mineral Assemblages From XRD

Locality	Tephra	Sample	Depositional Environment[a]	Max Intensity cps[b]	Amorphous	Smectite	Phillipsite	Chabazite	Analcite	Anorthoclase	K-spar	Jarosite	Calcite	Quartz	Erionite	Unidentified	Jarosite[c] (%)
Loc 40	IF	02-T103	Wetland	33	XXX	+	–	–	–	+	–	–	–	–	–	–	
Loc 41	IF	02-T118	Wetland	42	XXX	+	–	–	–	+	–	–	–	–	–	–	
Loc 39	IF	06-T64	Wetland/distal	44	XXX	X	X	–	–	+	–	–	–	–	–	–	
Loc 41	IF	02-T117	Wetland	42	XXX	+	–	–	–	+	–	–	–	–	–	–	
Loc 99	IF	01-T13	S Margin	88	XXX	+	–	–	–	X	–	–	–	–	–	–	
Loc 38	IF	02-T120	Distal margin	180	X	XX	–	+	X	+	–	–	–	–	–	–	
Loc 38	IF	02-T124	Distal margin	115	X	XXX	–	–	X	+	–	–	–	–	–	–	
Loc 38	IF	02-T123 y	Distal margin	142	X	XXX	X	XX	X	+	–	–	–	–	–	–	
Loc 38	IF	02-T123 g	Distal margin	95	XX	XXX	X	X	+	+	–	–	–	–	–	–	
Loc 38	IF	02-T122	Distal margin	145	–	XXX	XXX	XX	XX	+	–	–	–	–	–	–	
Loc 45	IF	06-T1	Proximal margin	175	X	XX	XXX	XXX	XX	+	–	–	–	–	–	–	
Loc 20	IF	06-T66	Proximal margin	175	X	X	XXX	XX	XX	+	–	–	XX	–	–	–	
Loc 44	IF	06-T92	Proximal margin	102	–	+	XX	XX	–	+	–	–	–	–	–	–	
Loc 42	IF	06-T4	Proximal margin	235	X	X	XXX	XXX	XX	+	–	–	–	–	–	–	
Loc 85	IF	06-T93	Proximal margin	230	–	X	XXX	XXX	–	+	–	–	–	–	–	–	
Loc 91	IF	06-T57	Intermittent	340	X	X	XXX	–	X	+	–	–	–	–	–	–	
Loc 88	IF	06-T41	Intermittent	320	X	XX	XXX	–	X	+	–	–	–	–	–	–	
Loc 46	IF	02-T133	Intermittent	290	–	XX	XXX	X	X	+	–	–	–	–	–	–	
Loc 80	IA	99-80-1A	Lake	510	–	XX	XX	XX	XX	+	–	–	XXX	–	–	–	
Loc 80	IB	99-802-1B	Lake	300	–	X	XXX	–	–	XX	XXX	X	–	–	–	–	2.60
Loc 80	below ID	99-802-22.5	Lake	270	–	X	XX	–	+	XX	XX	–	XXX	–	–	–	
Loc 80	ID	99-802-1D	Lake	580	–	+	XXX	–	+	XXX	+	–	–	–	–	–	
Loc 80	Ng'eju	99-802-1Em	Lake	660	–	+	XX	–	X	XXX	XX	–	–	–	–	–	
Loc 80	Ng'eju	99-802-1Eb	Lake	500	–	+	XXX	–	–	XX	X	–	–	–	–	–	
Loc 80	Ng'eju	99-802-1Et	Lake	330	–	X	XXX	–	–	XXX	X	–	–	–	–	–	
Loc 80	IF	06-T80	Lake	250	–	X	XXX	–	X	+	XX	XX	–	–	–	–	4.48
Loc 80	below IF	06-T85	Lake	487	–	XX	+	–	XXX	–	X	–	XXX	–	–	–	
Loc 80	below IF	06-T86	Lake	245	–	XX	XX	–	XXX		XX	–	–	–	–	–	
Loc 80	IF	08-T1	Lake	300	–	X	XXX	–	+	+	XXX	–	–	–	–	–	
Loc 80	IF	08-T2	Lake	340	–	X	XX	–	X	XXX	X	–	–	–	–	–	
Loc 80	IF	08-T3b	Lake	500	–	X	XX	–	X	XXX	X	–	–	–	–	–	
Loc 80	IF	08-T3T	Lake	250	–	–	XXX	–	+	XX	X	–	–	–	–	–	
Loc 80	IF	08-T4	Lake	250	–	X	XXX	–	X	+	XX	+	–	–	–	–	0.69
Loc 80	IF	08-T5	Lake	500	–	–	XX	–	X	XXX	XX	–	–	–	–	–	
Loc 80	IF	09-T23	Lake	252	–	X	XXX	–	X	+	XX	+	–	–	–	–	0.29
Loc 80-E	IF	08-T6	Lake	410	–	X	+	–	+	XXX	XX	X	–	–	–	–	2.77
Loc 80-E	IF	08-T7	Lake	340	–	X	xxx	–	X	XXX	XXX	–	–	–	–	–	
Loc 80-E	IF	08-T8	Lake	460	–	X	XXX	–	+	XXX	XX	–	–	–	–	–	
Loc 80-E	IF	08-T9	Lake	250	–	X	XXX	–	+	XX	X	–	–	–	–	–	
Loc 80-E	IF	08-T10	Lake	300	–	X	XXX	–	+	X	XX	–	–	–	–	–	

Table 1. (continued)

Locality	Tephra	Sample	Depositional Environment[a]	Max Intensity cps[b]	Amorphous	Smectite	Phillipsite	Chabazite	Analcite	Anorthoclase	K-spar	Jarosite	Calcite	Quartz	Erionite	Unidentified	Jarosite[c] (%)
Loc 80-W	IF	08-T11	Lake	250	−	X	XXX	−	+	X	XX	+	−	−	−	−	0.39
Loc 80-W	IF	08-T12	Lake	460	−	−	XXX	−	+	XXX	XX	−	−	−	−	−	
Loc 77	IF	08-T33	Lake	600	−	−	XXX	−	−	XXX	XX	−	−	−	−	−	
Loc 77	IF	08-T34	Lake	300	−	X	XXX	−	−	XXX	X	+	−	−	−	−	0.55
Loc 77	IF	08-T35	Lake	340	−	X	XX	−	−	XXX	XX	+	−	−	−	−	0.74
Loc 77	IF	08-T36	Lake	310	−	x	XXX	−	+	XXX	XX	−	−	−	−	−	
Loc 78	IF	08-T49	Lake	420	−	X	XXX	−	X	XX	XX	−	−	−	−	−	
Loc 78	IF	08-T50	Lake	390	−	+	XXX	−	+	XXX	X	−	−	−	−	−	
Loc 78	IF	08-T51	Lake	330	−	+	XXX	−	X	XXX	X	X	−	−	−	−	1.03
Loc 78	IF	08-T52	Lake	480	−	X	XXX	−	+	XXX	XX	+	−	−	−	−	0.15
Loc 54	IB	02-T9	Lake	317	−	+	X	−	+	X	XXX	−	−	−	−	−	
Loc 54	IE	02-T11	Lake	427	−	X	XX	−	−	XXX	XX	−	−	−	−	XXX	
Loc 54	Ng'eju	02-T12	Lake	1038	−	+	XX	−	−	XXX	XX	−	+	−	X	X	
Loc 54	Ng'eju	02-T13	Lake	1066	−	X	−	−	−	XXX	XXX	−	−	−	−	XX	
Loc 54	below IF	02-T14	Lake	1906	−	+	XXX	−	−	XXX	XX	−	−	−	−	XX	
Loc 54	IF	02-T15	Lake	365	−	X	XXX	−	−	XXX	XX	−	−	−	−	−	
Loc 54	IF	02-T16	Lake	341	−	XX	+	−	−	XXX	XXX	−	−	−	−	−	
Loc 54	IF	02-T17	Lake	410	−	X	XX	−	X	XXX	XX	+	−	−	−	−	0.49

[a]Depositional environment relates to Pleistocene sediments, and not to modern conditions. Tephra names are after *Hay* [1976]; tephra IDs are after *McHenry* [2005]. XXX, abundant; XX, common; X, rare to common; +, rare; −, absent.

[b]Percent jarosite calculated by Rietveld refinement (excluding clay minerals and amorphous); blank, 0%.

[c]Intensity above background of most intense peak.

rerun at 4 s per 0.01° 2θ to help separate potential minor jarosite peaks from background. Jarosite-bearing XRD patterns were further analyzed by Rietveld refinement using Bruker's TOPAS software and structure library to determine the jarosite concentration. The relative abundances of other minerals were determined qualitatively and categorized as abundant (highest peaks in the XRD pattern), common (prominent peaks, but not the highest), rare to common (easily identified peaks), rare (peaks recognizable), and absent (not identified).

3.3. X-Ray Fluorescence Analyses

[17] Select powdered samples were prepared and analyzed for major elements using a Bruker S4 Pioneer XRF spectrometer. 1.000 g of each sample was combined with 10.000 g of a 50/50 LiT/LiM flux with an integrated nonwetting agent and ~1 g of ammonium nitrate (oxidizer) and then fused in a Claisse M4 fluxer following the methods of *McHenry* [2009]. Additionally, 10 g of three jarosite-bearing powdered samples were milled with a wax binder and pressed at 30 tons of pressure for 1 min into 40 mm pressed pellets. The fused beads were analyzed for major elements (except S) using a calibration curve based on 11 USGS rock standards [*McHenry*, 2009], and the pressed pellets were analyzed for sulfur using a calibration curve based on 6 USGS rock standards. Loss on Ignition was determined by heating a dried, powdered sample in a muffle furnace at 1050°C for 15 min.

3.4. Electron Probe Microanalysis

[18] A thin section for sample 06-T80 (Locality 80) was prepared and analyzed by EPMA (Cameca SX 50) to determine the jarosite's chemical composition. The instrument was operated at 15 kV and 6 nA, with some analyses conducted using a focused beam and others using a beam defocused to 10 μm. The instrument was calibrated using sulfate and silicate standards. The small grain size (<1 μm) made it impossible to quantitatively measure the composition of a single crystal, though the jarosite crystals occur in overlapping clusters. Low totals likely indicate void space between adjacent crystals.

3.5. Scanning Electron Microscopy

[19] The same thin section used for EPMA was also imaged using a Hitachi S-3400 (SEM) to assess the context of the jarosite in relation to the zeolites. Minerals were identified qualitatively using Energy-Dispersive X-ray Spectrometry (EDS). An unpolished butt of sample 06-T80 was also examined using a Hitachi S-570 SEM to observe the crystal shapes and textural relationship between the jarosite and phillipsite. EDS was also used to qualitatively determine the composition of the jarosite.

3.6. Near-Infrared Methods

[20] Fourier Transform Infrared Reflectance (FTIR) spectra were taken using a Nicolet 6700 Smart Diffuse spectrometer with N_2 purge gas to remove atmospheric gases (H_2O and CO_2). NIR spectra were recorded in reflectance mode in the range of 200–12,500 cm^{-1} (0.8–5.0 μm) with a resolution of 4 cm^{-1}, although we subsampled the 1.0–2.6 μm range so that the data could be more easily compared to Observatoire pour la Mineralogie, l'Eau, les Glaces et l'Activité (OMEGA) and CRISM data available in the literature. The configuration used a quartz-halogen IR source, a CaF_2 beam splitter, and a DTGS detector. Background spectra using a Spectralon white standard were systematically taken before each sample's spectra to remove instrumental signal.

3.7. Mössbauer Methods

[21] Powdered samples prepared for XRD analyses were also used for Mössbauer analyses. A total of 15 samples were investigated, including samples from the paleowetland (02-T103); the distal paleolake margin (02-T122; 02-T124), intermittent (06-T41) and proximal paleolake margin (06-T93); and the paleolake center (99-802-1B; 02-T17; 08-T4; 08-T6; 08-T11; 08-T17; 08-T34; 08-T35; 08-T51; 08-T52). All samples identified as jarosite-bearing by XRD were also investigated by Mössbauer spectroscopy (except for 09-T23). Mössbauer spectra were obtained at room temperature with laboratory copies of the MER MIMOS instruments [*Klingelhöfer et al.*, 2003], which are set up in backscattering geometry. The Mössbauer source was ^{57}Co in Rh matrix. Spectra were evaluated analogous to Martian spectra, as described by *Morris et al.* [2006a, 2006b]. Area ratios are f-factor corrected to account for differences in recoil-free fractions (f(Fe3+)/f(Fe2+) = 1.21). Mössbauer parameters are quoted relative to α-Fe^0. Five of the samples were analyzed across a wider velocity (i.e., energy) range of approximately ±11 mm/s to scan for the presence of sextet phases typical for iron oxides such as hematite. Because there was no evidence for such in these five spectra, the remainder of the samples was investigated over a smaller velocity range of approximately±6 mm/s to increase the resolution for the central doublets in the spectra.

4. Results

4.1. XRD

[22] The XRD results for all samples are provided in Table 1. Eleven of the 55 samples analyzed by XRD have jarosite peaks above background. Rietveld refinement yielded concentrations for jarosite between 0.15 and 4.5% for these samples. All jarosite-bearing samples came from altered tephra in the central paleolake basin. The three samples collected from the same part of Tuff IF at Locality 80 in three separate visits (July or August 2006 (06-T80), 2008 (08-T4), and 2009 (09-T23)) all contained jarosite, but in different abundances.

[23] The rest of the mineral assemblage for the central paleolake basin samples consisted of anorthoclase (the dominant mineral in the fresh tephra, $(Na, K)AlSi_3O_8$), the zeolite mineral phillipsite, authigenic K-feldspar, and minor analcime and smectite. Relative abundances of these phases varied between sites and between samples from the same site, especially in the content of volcanic anorthoclase phenocrysts, the abundance of which varies depending on the specific part of the tephra sampled. Samples outside of the central paleolake basin lack jarosite and authigenic K-feldspar, instead containing an assemblage of phillipsite, chabazite ($(Ca, Na_2, K_2, Mg)Al_2Si_4O_{12} \cdot 6H_2O$), minor analcime, and more abundant smectite. The paleolake margin samples contain more smectite, with minor zeolites

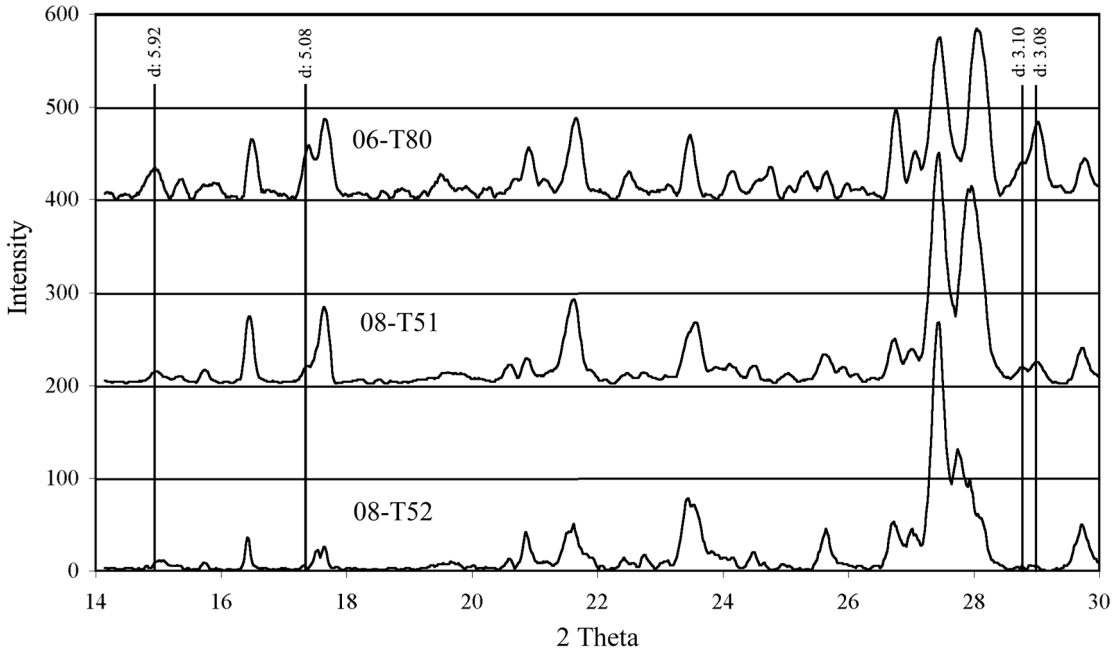

Figure 3. XRD patterns for samples 06-T80, 08-T51, and 08-T52, 2θ 14–30°. Sample 06-T80, from Locality 80, contains abundant jarosite (solid lines, with d-spacings in Å) in a sample predominantly composed of phillipsite and K-feldspar and containing smectite and minor analcime and anorthoclase. Sample 08-T51, from Locality 78, is similar except for its lower jarosite content. Sample 08-T52, also from Locality 78, contains only minor jarosite and less phillipsite.

and no jarosite. A more detailed account of the authigenic mineralogy across the paleolake basin is provided by *McHenry* [2009, 2010]. Three XRD plots, for samples 06-T80 (jarosite-rich), 08-T51 (minor jarosite) and 08-T52 (trace jarosite) are provided in Figure 3.

[24] The exact identity of the clay minerals was not investigated in detail in this study, but qualitative EDS analysis reveals that they are Mg- and Fe-rich and FTIR reflectance identified an Al-Fe smectite, possibly an Al-rich nontronite ($Na_{0.3}Fe^{3+}{}_2(Si, Al)_4O_{10}(OH)_2 \cdot nH_2O$). Previous work by *Hover and Ashley* [2003] found Mg-rich trioctahedral smectite (stevensite, $(Ca, Na)_x(Mg, Fe^{2+})_3Si_4O_{10}(OH)_2$) in the paleolake margin and neoformed celadonite ($K(Mg, Fe^{2+})(Fe^{3+}, Al)(Si_4O_{10})(OH)_2$) in the paleolacustrine sediments, but their study did not focus exclusively on altered tephra. *Hay and Kyser* [2001] also conducted detailed clay mineralogical analysis of these deposits and did not assign a specific mineral name to the Mg-rich lacustrine smectite. The XRD pattern for sample 06-T80 is consistent with celadonite or glauconite ($(K, Na)(Fe^{3+}, Al)(Mg, Fe^{2+})(Si, Al)_4O_{10}(OH)_2$) [*McHenry*, 2010], but other samples (including 02-T17) have clay peaks more consistent with montmorillonite or other clays (Table 1), and the FTIR and Mössbauer results suggest nontronite or celadonite. The geochemical results that follow indicate much higher Fe than Mg concentrations, which could indicate a more Fe-rich (as opposed to Mg-rich) clay phase, which would be consistent with celadonite, nontronite, or an Fe-rich smectite. This is also supported by qualitative EDS analysis of clay-rich parts of the thin sections, which show abundant Fe and lower Mg abundances.

4.2. XRF Results

[25] Major element compositions for many of the non-jarosite-bearing samples are reported by *McHenry* [2009]. Compositions for samples 06-T80, 08-T4, and 09-T23, including sulfur, are reported in Table 2. These three samples were collected within centimeters of each other at the same site during July-August (the dry season) in three different years, yet show different bulk compositions, primarily in their Fe_2O_3 and SO_3 content and LOI values, mirroring the differences in their XRD patterns.

4.3. EPMA Results

[26] Jarosite compositions, as determined by EPMA, are presented in Table 2. Totals (not including water, with oxygen determined stoichiometrically) were between 80 and 85%, with differences in both SO_3 and Fe_2O_3 accounting for the range of totals. Detailed inspection of the EDS spectra did not reveal any potential contributions from unanalyzed elements. Assuming that the low totals are the result of void space or excess water, some preliminary interpretation of the composition of the jarosite is possible. First, substitution of Al^{3+} for Fe^{3+} is present but not major, with concentrations of Al_2O_3 of up to 4.2% in a sample with over 39% Fe_2O_3. Na^+ substitution for K^+ is also minor, with Na_2O concentrations of 0.2–0.9% compared to 8.2–8.5% K_2O. The jarosite is thus K-rich.

4.4. SEM Results

[27] SEM analysis of sample 06-T80 from Locality 80 revealed abundant phillipsite and K-feldspar, minor analcime, and clusters rich in jarosite (Figure 2). Jarosite clusters were lined by clay or directly adjacent to clusters of phil-

Table 2. Geochemical Results[a]

Sample	SiO_2	TiO_2	Al_2O_3	Fe_2O_3	MnO	MgO	CaO	Na_2O	K_2O	P_2O_5	SO_3	LOI	SUM
XRF Results													
06-T80	54.70	0.27	14.60	7.32	0.01	0.68	0.16	4.12	8.05	0.05	1.72	9.54	101.23
08-T4	55.81	0.31	15.43	6.29	0.02	0.85	0.37	3.80	8.59	0.06	1.02	5.87	98.42
09-T23	61.03	0.33	15.89	4.32	0.01	0.95	0.21	4.13	8.79	0.05	0.15	6.09	101.95
EPMA Results													
06-T80-1	0.39		2.83	41.76	0.04	0.07		0.88	6.60		32.08		84.64
06-T80-2	0.82		3.21	38.71	0.03	0.10		0.24	8.42		29.84		81.36
06-T80-3	1.72		2.88	37.40	0.01	0.17		0.35	8.25		29.44		80.20
06-T80-4	0.71		3.37	40.70	0.00	0.10		0.15	8.25		29.83		83.10
06-T80-5	0.61		2.71	38.73	0.03	0.05		0.32	8.47		29.68		80.60
06-T80-6	0.78		3.94	38.40	0.04	0.16		0.24	8.37		29.73		81.65
06-T80-7	1.70		3.59	37.48	0.00	0.27		0.26	8.40		28.87		80.56
06-T80-8	1.26		4.14	39.42	0.00	0.16		0.25	8.23		29.25		82.67
Average (n = 8)	1.00		3.33	39.07	0.02	0.13		0.33	8.12		29.84		81.85
StDev	0.50		0.53	1.51	0.02	0.07		0.23	0.62		0.96		1.53

[a]XRF compositions are of Locality 80 jarosite-bearing samples, and EPMA compositions are of Locality 80 jarosite (sample 06-T80).

lipsite or K-feldspar laths. The jarosite crystals were consistent in size across all clusters examined, typically around 1 μm. Qualitative EDS analysis on the jarosite crystals revealed abundant S, K, and Fe, with minor Al. Minor Si in some analyses can likely be attributed to overlap with adjacent clays or K-feldspar or phillipsite laths.

4.5. NIR Results

[28] The FTIR spectra of the two analyzed samples (06-T80 and 99-802-1B, both from Locality 80) show a clear smectite signal, with the two characteristic hydration bands at 1.4 and 1.9 μm. These two bands are associated with water and hydroxyl groups in smectites and in zeolites. The clear band at 2.30 μm is due to the Fe-OH bond in the smectite, while the weaker band at 2.21 μm is due to Al-OH in the structure (Figure 4). Thus the FTIR results confirm the presence of an Al, Fe^{3+}-smectite, likely a nontronite. Jarosite is identified by four weak bands at 1.46, 1.85, 1.92 and 2.26 μm (there are several other minor bands). The FTIR spectra exhibit a weak absorption band at 1.8 μm and several "humps" in other larger bands, at 1.46, 1.96 and 2.26 μm. The very weak bands confirm that jarosite is a minor phase and that the NIR spectrum is essentially dominated by smectite, although since the band depth is dependent on the optical constant, jarosite could be more abundant if its optical constants are weaker than those of smectite.

4.6. Mössbauer Results

[29] Fifteen samples were investigated with Mössbauer spectroscopy, ten of which contained jarosite detected by XRD. A doublet corresponding to Fe^{3+} in jarosite could be identified in the Mössbauer spectra of all ten of these samples (Figure 5 and Data Sets 1 and 2).[1] A second doublet is present in all fifteen samples and is consistent with Fe^{3+} in dioctahedral phyllosilicates such as glauconite, celadonite and/or nontronite [*Daynyak and Drits*, 1987; *Reid et al.*, 1988; *Bowen et al.*, 1989; *Drits et al.*, 1997]. It is possible that nanophase, i.e., superparamagnetic Fe (hydr)oxides contribute to this doublet. Nanophase oxyhydroxides have been identified in claystones from this location by *Hover and Ashley* [2003]. The sextet identified in sample 08-T34 is also consistent with an Fe-(oxyhydr)oxide, possibly superparamagnetic or Al-substituted goethite (α-FeOOH). These

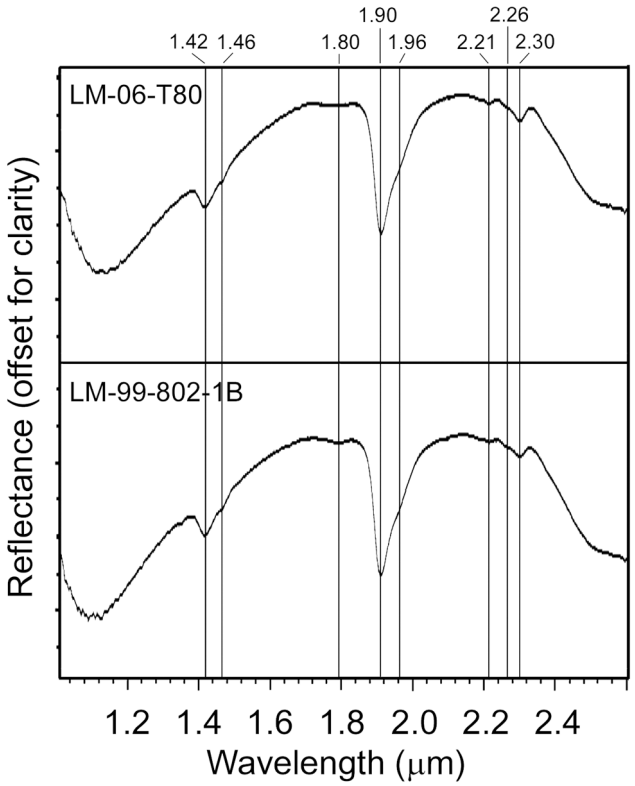

Figure 4. The FTIR spectra show two characteristic smectite hydration bands at 1.4 and 1.9 μm, a clear band at 2.3 μm due to the Fe-OH bond, and a weaker band at 2.2 μm due to Al-OH in the structure, indicating an Al, Fe^{3+}-smectite, likely nontronite. Jarosite is identified by four major bands at 1.46, 1.85, 1.92 and 2.26 μm. A weak absorption band at 1.8 μm and several "humps" in other larger bands at 1.46, 1.96 and 2.26 μm are consistent with jarosite as a minor phase.

[1]Auxiliary materials are available at ftp://ftp.agu.org/apend/je/2010je003680.

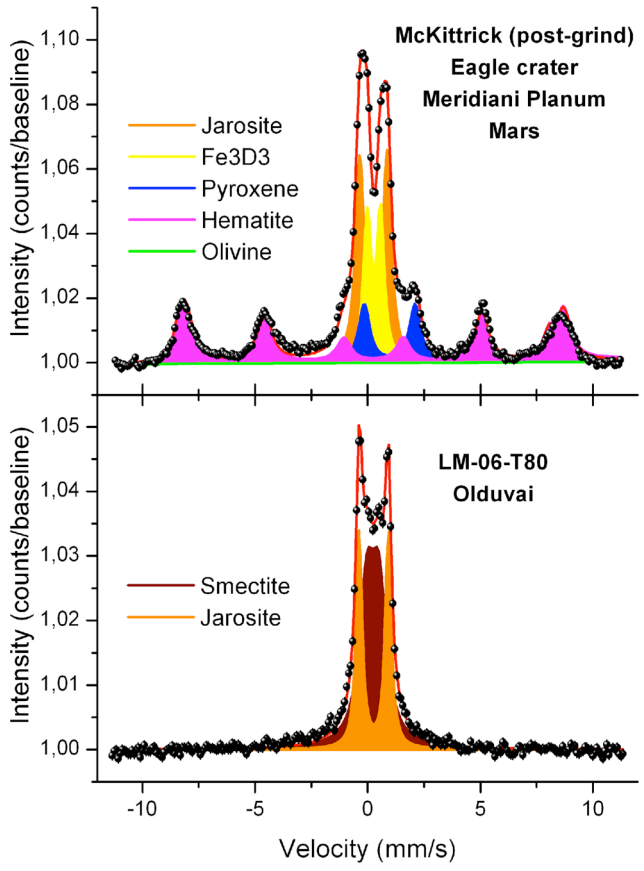

Figure 5. Comparison of (top) a typical Meridiani Planum, Mars, sulfate-rich evaporitic outcrop spectrum with (bottom) a jarosite-rich sample from Olduvai Gorge. Both spectra show two central ferric doublets, jarosite and an unidentified phase designated as Fe3D3 in the Meridiani spectrum [*Klingelhöfer et al.*, 2004; *Morris et al.*, 2006b], and jarosite in combination with a ferric smectite and/or nanophase iron oxides in the Olduvai spectrum. Possible phases for Fe3D3 include the superparamagnetic forms of hematite and goethite, ferrihydrite, akaganeite, and schwertmannite or perhaps a phyllosilicate. The Meridiani spectrum shows additional phases, two ferrous doublets identified as pyroxene and olivine by *Klingelhöfer et al.* [2004] and *Morris et al.* [2006b], and the iron oxide hematite. Hematite occurs both in the matrix of the sedimentary rock and in the form of late diagenetic mm-sized spherules, dubbed "blueberries."

phases would not be detected by XRD. Nontronite is a ferric mineral, celadonite and glauconite are mixed-valence Fe minerals distinguished on the basis of their Al content. The remaining doublets in the Mössbauer spectra are consistent with Fe^{2+} in these minerals [*Daynyak and Drits*, 1987; *Reid et al.*, 1988; *Bowen et al.*, 1989; *Drits et al.*, 1997] or possibly stevensite. *Reid et al.* [1988] and *Bowen et al.* [1989] documented the pedogenic alteration of celadonite into an Fe-rich smectite upon the release of interlayer K^+ ions. These K^+ ions would then be available for the formation of jarosite. Olduvai jarosite has average values for δ of 0.37 mm/s and ΔE_Q of 1.30 mm/s. Jarosite ΔE_Q increases from H_3O^+ to Na^+ to K^+ as dominant cation [*Leclerc*, 1980] and with Al^{3+} for Fe^{3+} substitution [*Morris et al.*, 2006b]. The ΔE_Q of Olduvai jarosite is consistent with K^+ as the dominant monovalent cation and possible Al^{3+} for Fe^{3+} substitution.

[30] Samples from the wetland and distal lake margin paleoenvironments have a higher abundance of ferrous doublets and therefore lower Fe^{3+}/Fe_{Total} ratios (0.41–0.58) than the intermittent to proximal lake margin or the lake center paleoenvironments. The Fe^{3+}/Fe_{Total} ratios of jarosite-bearing paleolake center samples vary between 0.78 and 1.00, showing a predominance of ferric phases, whereas the intermittent and proximal paleolake margin samples (that do not contain jarosite) are both almost completely oxidized (both 0.98). Jarosite abundance and Fe^{3+}/Fe_{Total} ratios thus do not correlate (Data Sets 1 and 2 and Figure 6), indicating that it is not just the presence of oxidized iron that determines the presence or absence of jarosite.

4.7. Modern Groundwater

[31] Modern groundwater in the Olduvai basin and particularly near the jarosite-bearing exposures (e.g., springs at Locality 78) is saline-alkaline, with trona being actively

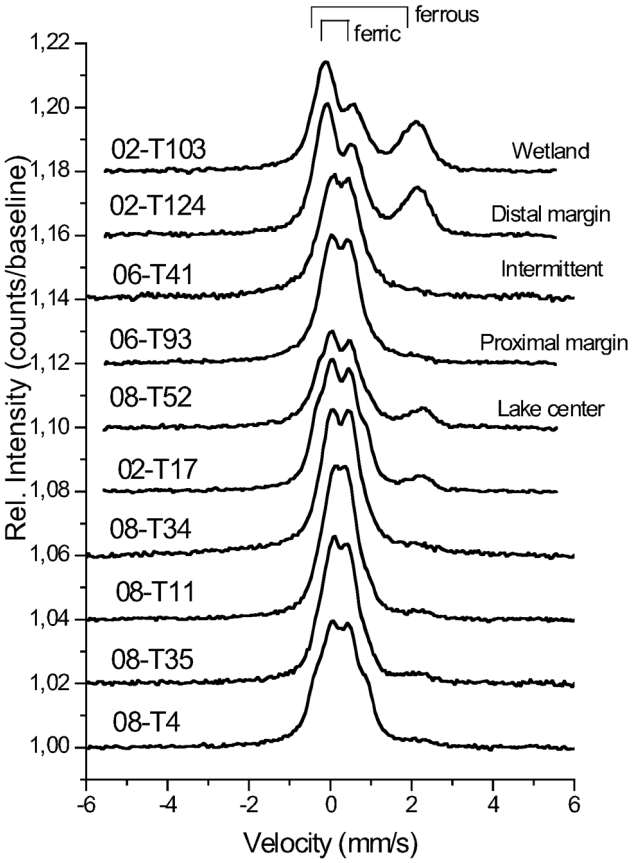

Figure 6. Comparison of Mössbauer spectra of Olduvai samples, starting from (top) paleowetland and distal paleolake margin samples toward (bottom) the paleolake center. Ferrous phases are more abundant in samples from the distal lake margin relative to the paleolake center, but Fe^{3+}/Fe_{Total} ratios within the paleolake center vary. Bars at the top are a rough guide to where ferrous and ferric doublet lines appear in the spectra. All spectra are composed of more than one overlapping ferric and/or ferrous doublets.

precipitated where it emerges. This is consistent with high pH (9–10) and Na-bicarbonate dominated water [*Hay*, 1964], and is inconsistent with what is currently known about jarosite stability. The pH (9.29 and 9.54) and conductivity (14.6 and 25.6 mS) for two of these springs were measured in the field in 2009 at 17.5°C.

5. Discussion

5.1. Comparison of Results From Different Methods

[32] XRD, EPMA, SEM, Mössbauer, and FTIR analysis all confirmed the presence of jarosite in some samples. Ten of the samples with and five without jarosite as detected by XRD were analyzed by Mössbauer. These two analytical techniques agree, as jarosite was detected in all ten XRD-confirmed jarosite-bearing samples and in none of the five other samples. The composition of the jarosite derived from the different analytical methods is also consistent: when compared to jarosite patterns in the ICDD database, the XRD patterns are most consistent with patterns of K-rich jarosite (as opposed to Na- or H-rich jarosite), the qualitative EDS (SEM) and quantitative EPMA compositional analysis of the jarosite in sample 06-T80 also shows a high K content, and the Mössbauer results are also consistent with K^+ as the dominant cation. Both the EPMA compositional analysis and Mössbauer results are consistent with small amounts of Al^{3+} for Fe^{3+} substitution in the jarosite. In this study, the different analytical methods thus agree on the presence/absence and composition of jarosite.

5.2. Jarosite Distribution

[33] The eleven jarosite-bearing samples came from all four sampled sites within the central lake basin paleoenvironment. No jarosite was observed in the intermittently dry lacustrine, proximal or distal lake margin, or wetlands paleoenvironment samples. Not all central lake basin paleoenvironment samples yielded jarosite, and jarosite content varied even within a single tephra exposure and between samples collected from the same exposure in different years.

[34] The jarosite-bearing samples vary only slightly in the rest of their authigenic assemblages. Phillipsite and K-feldspar dominate, though their relative abundances vary. Smectite and analcime are also present, at least in minor amounts, in all jarosite-bearing Tuff IF samples. The abundance of anorthoclase, the dominant phenocryst in the unaltered tephra, varies between samples depending on the original crystal content of that part of the tephra. The authigenic assemblages of the non jarosite-bearing samples from the central lake basin paleoenvironment are similar to those of the jarosite-bearing samples (phillipsite, K-feldspar, analcime, anorthoclase), but some of them contain more clay. None of the jarosite-bearing samples contain abundant clay.

[35] The three samples collected from the jarosite-rich layer of Tuff IF at Locality 80 in three separate years (samples 06-T80, 08-T4, and 09-T23) all contained jarosite (4.5%, 0.7%, and 0.3%, respectively). Sample 09-T23 also contains less SO_3 and Fe_2O_3 in its bulk composition, while the concentrations of other elements remain unchanged. This apparent year-to-year change in jarosite abundance within a small area of the same exposure could be attributed either to heterogeneous distribution of jarosite on the centimeter scale, or to an ephemeral or seasonal jarosite occurrence. Unfortunately, the exact cause cannot be determined based on the limited samples collected.

5.3. Potential Formation Pathways

[36] Potential explanations for the cooccurrence of jarosite and alkaline zeolite minerals include precipitation of jarosite in modern acidic groundwater passing through zeolite deposits, a physical mixture between acidic and alkaline mineral assemblages, or local oxidation of pyrite. These models are all discussed in the following section, though the local oxidation of pyrite is the preferred explanation for the Olduvai deposit.

5.3.1. Direct Precipitation in Modern or Ancient Groundwater

[37] One possible explanation for this occurrence would be the direct precipitation of jarosite either at the time of deposition, or as modern groundwater percolated through the deposit. However, the alkaline (pH > 9) mineral assemblage of the sedimentary deposit requires conditions far outside the accepted stability field of jarosite. The modern groundwater has a similar high pH (as measured at two springs in the central paleolake basin), making jarosite an unlikely precipitate. Instead, efflorescences of Na bicarbonate minerals (such as trona) precipitate at the modern springs.

5.3.2. Physical Mixture of Acidic and Alkaline Components

[38] Another possibility is that jarosite and phillipsite are found together as part of a physical mixture between alkaline zeolite-bearing sediments and acidic jarosite-bearing sediments. However, the close textural association of the two minerals (Figure 2) makes this potential origin unlikely. Additionally, the samples derive from the interior of a layered tephra deposit with no evidence of mixing with other sediments after deposition. The similarity of the volcanic mineral assemblage between Locality 80 and other exposures of Tuff IF within and outside of the lacustrine deposit [*McHenry*, 2005; *McHenry et al.*, 2008] also suggests that this sample is not detritally contaminated. There is also no known potential source for detrital jarosite within the Olduvai Basin.

5.3.3. Late-Stage Formation as a Result of Pyrite Oxidation

[39] A more plausible mechanism for the formation of this deposit is the oxidation of pyrite. *Hay* [1973] and *Hay and Kyser* [2001] identified altered pyrite within the Olduvai paleolake sediments. Such pyrite could have formed early during diagenesis, in association with zeolites. In this model, phillipsite and K-feldspar formed in tephra altered in the high-pH ground and lake water following deposition. Pyrite could have formed soon after deposition as water containing dissolved sulfate underwent reduction by organic matter:

$$2CH_2O + SO_4^{2-} = 2HCO_3^- + H_2S$$

H_2S then reacted with Fe^{2+} in the muds (available after Fe^{3+} reduction of detrital ferric oxides or clay minerals undergoing dissolution-precipitation processes), forming pyrite, a mechanism suggested by *Hay and Kyser* [2001].

Table 3. Comparison of Martian and Olduvai Igneous Precursor Compositions[a]

Site	Sample	SiO_2	TiO_2	Al_2O_3	Fe_2O_3T	MnO	MgO	CaO	Na_2O	K_2O	P_2O_5	Sum
Gusev	Adirondack[b]	45.30	0.49	10.42	19.34	0.42	11.90	7.76	2.09	0.03	0.54	98.29
Meridiani	OCBP1[c]	48.19	1.01	8.06	20.75	0.43	10.40	6.46	2.19	0.75	1.37	99.61
Olduvai	02-T103[d]	62.70	0.67	17.28	6.24	0.20	1.87	1.39	6.18	3.35	0.12	100.00

[a]Note: concentrations only reported for elements measured at all three sites.
[b]Extrapolated end-member chemical composition for Adirondack, Gusev [*McSween et al.*, 2006].
[c]Extrapolated outcrop precursor basalt, Meridiani [*Morris et al.*, 2006b].
[d]Bulk fresh Tuff IF lapilli composition, Locality 40, Olduvai, normalized to 100% [*McHenry*, 2009].

[40] More recently, perhaps in modern groundwater, pyrite was oxidized:

$$FeS_2 + 15/4\ O_2 + 7/2\ H_2O = Fe(OH)_3 + 2H_2SO_4$$

[after *Bigham and Nordstrom*, 2000]. The sulfuric acid locally lowered the pH into the jarosite stability field. It is also possible that the pyrite oxidized directly into jarosite, rather than through an intermediate iron hydroxide mineral [e.g., *Courtin-Nomade et al.*, 2009]. Jarosite can also be formed by the evaporation of pyrite weathering fluids upon exposure [e.g., *Tuttle and Breit*, 2009]. Either way, pH would be locally lowered. The acidic conditions caused by the oxidation of pyrite did not persist long enough to destroy the phillipsite, and were not widespread enough to modify the overall groundwater regime. It should be noted that no pyrite has been directly observed in samples collected for this study, though altered pyrite from this deposit has been previously described [*Hay and Kyser*, 2001] and rust-lined cubic holes (likely pseudomorphs after pyrite) were observed in the surrounding claystone during a brief visit to Locality 80 in 2010. The formation of jarosite is most likely recent, as the pH ~ 9.5 modern groundwater would destroy it over time. Jarosite decomposes readily into goethite under alkaline conditions [*Dutrizac and Jambor*, 2000]. Though goethite is not observed in the XRD patterns in the current study, Mössbauer spectra show an Fe-(oxyhydr)oxide in sample 08-T34, which had only a low jarosite content.

[41] This pyrite oxidation model is consistent with other nonacidic occurrences of jarosite, including the studies reported by *Ashley et al.* [2004], *Leveille* [2007], and *Darmody et al.* [2007] discussed in section 1.1. Pyrite oxidation processes thus appear to allow jarosite to form, even under outcrop-scale pH conditions that are far from this mineral's normal stability field.

5.4. Comparison to Martian Jarosite

5.4.1. Jarosite Composition

[42] The one place on Mars where jarosite has been analyzed in detail is Meridiani Planum. Mössbauer results for jarosite there have average values for the isomer shift δ of 0.37 mm/s and the quadrupole splitting ΔE_Q of 1.20 mm/s. Meridiani Planum jarosite thus has $Na^+ > K^+ > H_3O^+$ as monovalent cation with possible Al^{3+} for Fe^{3+} substitution [*Morris et al.*, 2006b]. APXS data [e.g., *Rieder et al.*, 2004] cannot confirm this, as this instrument cannot detect hydrogen, and some modeling results [e.g., *Clark et al.*, 2005] are consistent with hydronium jarosite. In contrast, the Olduvai jarosite is K-rich, as indicated by Mössbauer and EPMA results. While jarosite has not yet been detected from orbit at Meridiani Planum, *Milliken et al.* [2008] interpret their CRISM data from outcrops south of Ius/Melas Chasma as most consistent with hydronium jarosite and *Farrand et al.* [2009] interpret their CRISM data from the vicinity of Mawrth Vallis as most consistent with K-rich jarosite, more consistent with the Olduvai results.

5.4.2. Different Starting Compositions

[43] The composition of the starting material was also very different at Olduvai compared to Meridiani Planum on Mars. At Olduvai, the initial material prior to alteration was trachytic to phonolitic volcanic ash, with a very alkaline composition. In contrast, the igneous rocks of Mars are overwhelmingly basaltic and dominated by Fe-rich tholeiitic compositions [e.g., *McSween et al.*, 2009]. Table 3 shows the differences in composition between fresh Tuff IF [*McHenry*, 2009] and extrapolated starting compositions of basalts at Meridiani (OCBP1) [*Morris et al.*, 2006b] and Gusev Crater (Adirondack) [*McSween et al.*, 2006]. Given these significant differences in starting composition, and the greater availability of sulfur at the Martian sites, it would not be expected to see the exact same mineral assemblages and geochemical pathways. The relative abundance of K in the Olduvai system allows for the development of K-rich minerals, including authigenic K-feldspar, phillipsite, and K-rich jarosite, while its near absence at Meridiani [*Rieder et al.*, 2004] and other Martian sites makes this assemblage unlikely. If zeolites were to form at Meridiani, Gusev, or elsewhere on Mars as an end result of basalt alteration, they would most likely be Ca-rich varieties more consistent with the general composition of Martian basalt.

5.4.3. Implications for Mars

[44] Jarosite has been detected at a few sites on Mars, and analyzed directly at Meridiani Planum where its presence is consistent with other indicators of acidity (including Mg sulfates [e.g., *Tosca et al.*, 2005]). Zeolites would likely be detectable by MiniThermal Emission Spectrometer (MiniTES) at Meridiani if they were abundant, and their absence is also consistent with acidic conditions. However, elsewhere on Mars the context of potential zeolites, sulfates, and Mg/Fe phyllosilicates is less well developed. *Ruff* [2004] predicted a significant zeolite component in Martian dust, and discrete occurrences of specific zeolites (e.g., analcime [*Ehlmann et al.*, 2009]) have been confirmed.

[45] The coexistence of jarosite and Fe/Mg phyllosilicates at Olduvai and in paleolakes on Mars is also important for determining the aqueous geochemical conditions at the time of deposition or diagenesis. Jarosite and many other Mg or Fe sulfates generally indicate acidic conditions, yet Fe/Mg phyllosilicates and zeolites are generally formed under alkaline or neutral conditions. While in most places on Mars there is a clear stratigraphic or temporal difference between Fe/Mg phyllosilicate-rich and sulfate deposits, both are

observed at an equivalent level at two small-scale exposures in Terra Meridiani [*Poulet et al.*, 2008]. *R. Wray et al.* [2009] also found a small exposure containing both jarosite and Fe/Mg phyllosilicates in Columbus Crater, a potential paleolake in Terra Sirenum. *Farrand et al.* [2009] describe a jarosite-rich layer directly overlying a Mg/Fe smectite-rich deposit in a potential paleolake environment in the vicinity of Mawrth Vallis, and postulate that the jarosite could have formed by later acid-sulfate alteration of the Mg/Fe smectite layers beneath [*Altheide et al.*, 2010]. These close associations between "acidic" and "alkaline" mineral assemblages on Mars are similar to that observed in the Olduvai paleolacustrine deposit, and suggest that pH conditions must have varied on a small scale during or following deposition [*Baldridge et al.*, 2009]. A long and sufficiently complex diagenetic history could include multiple episodes of water-rock interaction under different conditions, potentially allowing the coexistence of more alkaline (e.g., Mg/Fe phyllosilicate or zeolite) and more acidic (e.g., Fe sulfate) minerals at Olduvai or on Mars. It is therefore risky to use the presence of a single mineral (e.g., jarosite) as an indicator of the pH conditions of the deposit as a whole.

[46] Zeolites, Mg/Fe phyllosilicates, or other minerals forming at neutral to high pH, should not be excluded from consideration just because the presence of sulfate minerals (such as jarosite) suggests acidic conditions. Unfortunately, the difficulty of resolving certain zeolites from polyhydrated sulfate minerals using CRISM data [e.g., *J. J. Wray et al.*, 2009] currently limits our ability to determine the extent of zeolitic mineralization on Mars. The acidic conditions required to produce jarosite can be local and/or short-lived, and can post date the formation of the rest of the mineral assemblage. In addition, the apparent short lifetime of jarosite in Olduvai samples is promoted by the abundance of water and warm conditions, which allow fast reequilibration of the system [*Elwood Madden et al.*, 2009]. However, in the very dry and cold Martian climate, it is possible that jarosite would last much longer. On Mars, *Fairén et al.* [2009] have suggested that the jarosite observed by MER Opportunity was formed long after the rest of the assemblage, perhaps even within Amazonian times, and would therefore not be the best indicator of the conditions under which the overall deposit was formed. Due to the absence of water in Meridiani Planum since the formation of the deposit, the jarosite could have lasted for a very long time even if not stable.

6. Conclusions

[47] Jarosite occurs in altered tephra within lacustrine sediments of the Pliocene-Pleistocene Olduvai deposits, associated with saline-alkaline minerals. Olduvai was in the past and is still a saline-alkaline environment, thus any acidic conditions would have been minor, local, or of short duration. Pyrite oxidation could have produced small amounts of sulfuric acid, providing a local acidic environment capable of forming jarosite in a system otherwise dominated by highly alkaline minerals and groundwater. Under these conditions, jarosite is not a good indicator of dominantly acidic conditions.

[48] Olduvai jarosite is not a direct Mars analog since the original volcanic material was phonolitic, and the resulting authigenic mineral assemblage is dominated by K-rich phases (including jarosite) and lacks other sulfate minerals and hematite. However, it does demonstrate that alkaline conditions and zeolites, Mg/Fe phyllosilicates, or other minerals forming at neutral to high pH cannot be excluded from consideration because jarosite is present. Martian deposits with mixed Mg/Fe phyllosilicate and jarosite or other Mg, Fe sulfates such as the potential paleolake deposit at Columbus Crater/Terra Sirenum [*R. Wray et al.*, 2009] or Terra Meridiani [*Poulet et al.*, 2008] may represent complex diagenetic histories similar to that of the Olduvai deposit.

[49] **Acknowledgments.** The authors would like to thank present and past members of the Olduvai Landscape Paleoanthropology Project (OLAPP) for their field support, Lis Rushworth for the field pH and conductivity measurements of the Olduvai springs, and John Fournelle and Heather Owen for their help on the EPMA and SEM analyses. L.J.M. also thanks Richard Hay for introducing her to Olduvai tephra alteration. The authors would also like to thank G. Klingelhöfer for access to the MER-like Mössbauer spectrometers. This research was supported in part by funds from the UW Milwaukee Research Growth Initiative, American Chemical Society Petroleum Research Fund, L.S.B. Leakey Foundation, and National Science Foundation (BCS-0852292 to L.J.M.).

References

Altheide, T. S., V. F. Chevrier, and E. Z. Noe Debra (2010), Mineralogical characterization of acid weathered phyllosilicates with implications for secondary Martian deposits, *Geochim. Cosmochim. Acta*, *74*, 6232–6248, doi:10.1016/j.gca.2010.08.005.

Ashley, G. M., J. Maitima Mworia, A. M. Muasya, R. B. Owens, S. G. Driese, V. C. Hover, R. W. Renut, M. F. Goman, S. Mathai, and S. H. Blatt (2004), Sedimentation and recent history of a freshwater wetland in a semi-arid environment: Loboi Swamp, Kenya, East Africa, *Sedimentology*, *51*, 1301–1321, doi:10.1111/j.1365-3091.2004.00671.x.

Baldridge, A. M., S. J. Hook, J. K. Crowley, G. M. Marion, J. S. Kargel, J. L. Michalski, B. J. Thomson, C. R. de Souza Filho, N. T. Bridges, and A. J. Brown (2009), Contemporaneous deposition of phyllosilicates and sulfates: Using Australian acidic saline lake deposits to describe geochemical variability on Mars, *Geophys. Res. Lett.*, *36*, L19201, doi:10.1029/2009GL040069.

Benison, K. C., and D. A. LaClair (2003), Modern and ancient extremely acid saline deposits: Terrestrial analogs for Martian environments?, *Astrobiology*, *3*, 609–618, doi:10.1089/153110703322610690.

Bibring, J.-P., et al. (2007), Coupled ferric oxides and sulfates on the Martian surface, *Science*, *317*, 1206–1210, doi:10.1126/science.1144174.

Bigham, J. M., and D. K. Nordstrom (2000), Iron and aluminum hydroxysulfates from acid sulfate waters, in *Sulfate Minerals: Crystallography, Geochemistry, and Environmental Significance*, edited by C. N. Alpers, J. L. Jambor, and D. K. Nordstrom, pp. 351–403, Mineral. Soc. of Am., Washington, D. C.

Bishop, J. L., P. Schiffman, E. Murad, M. D. Dyar, A. Drief, and M. D. Lane (2007), Characterization of alteration products in tephra from Haleakala, Maui: A visible-infrared spectroscopy, Mössbauer spectroscopy, XRD, EMPA, and TEM study, *Clays Clay Minerals*, *55*, 1–17, doi:10.1346/CCMN.2007.0550101.

Bowen, L. H., E. DeGrave, D. A. Reid, R. C. Graham, and S. B. Edinger (1989), Mössbauer study of a California desert celadonite and its pedogenically related smectite, *Phys. Chem. Minerals*, *16*, 697–703, doi:10.1007/BF00223320.

Burns, R. G. (1986), Terrestrial analogues of the surface rocks of Mars?, *Nature*, *320*, 55–56, doi:10.1038/320055a0.

Burns, R. G., and D. S. Fisher (1990), Iron-sulfur mineralogy of Mars: Magmatic evolution and chemical weathering products, *J. Geophys. Res.*, *95*, 14,415–14,421, doi:10.1029/JB095iB09p14415.

Chevrier, V., P. Rochette, P.-E. Mathé, and O. Grauby (2004), Weathering of iron-rich phases in simulated Martian atmospheres, *Geology*, *32*, 1033–1036, doi:10.1130/G21078.1.

Chevrier, V., P.-E. Mathé, P. Rochette, O. Grauby, G. Bourrié, and F. Trolard (2006), Iron weathering products in a CO_2 + (H_2O or H_2O_2) atmosphere: Implications for weathering processes on the surface of Mars, *Geochim. Cosmochim. Acta*, *70*, 4295–4317, doi:10.1016/j.gca.2006.06.1368.

Clark, B. C., et al. (2005), Chemistry and mineralogy of outcrops at Meridiani Planum, *Earth Planet. Sci. Lett.*, *240*, 73–94, doi:10.1016/j.epsl.2005.09.040.

Courtin-Nomade, A., C. Grosbois, M. A. Marcus, S. C. Fakra, J.-M. Beny, and A. L. Foster (2009), The weathering of a sulfide orebody: Speciation and fate of some potential contaminants, *Can. Mineral.*, *47*, 493–508, doi:10.3749/canmin.47.3.493.

Darmody, R. G., C. E. Thorn, and J. C. Dixon (2007), Pyrite-enhanced chemical weathering in Kärkevagge, Swedish Lapland, *Geol. Soc. Am. Bull.*, *119*, 1477–1485, doi:10.1130/B26228.1.

Daynyak, L. G., and V. A. Drits (1987), Interpretation of Mössbauer spectra of nontronite, celadonite, and glauconite, *Clays Clay Minerals*, *35*, 363–372, doi:10.1346/CCMN.1987.0350506.

Drits, V. A., L. G. Dainyak, F. Muller, G. Besson, and A. Manceau (1997), Isomorphous cation distribution in celadonites, glauconites and Fe-illites determined by infrared, Mössbauer and EXAFS spectroscopies, *Clay Minerals*, *32*, 153–179, doi:10.1180/claymin.1997.032.2.01.

Dutrizac, J. E., and J. L. Jambor (2000), Jarosites and their application in hydrometallurgy, in *Sulfate Minerals: Crystallography, Geochemistry, and Environmental Significance*, edited by C. N. Alpers, J. L. Jambor, and D. K. Nordstrom, pp. 405–452, Mineral. Soc. of Am., Washington, D. C.

Ehlmann, B. L., et al. (2009), Identification of hydrated silicate minerals on Mars using MRO-CRISM: Geologic context near Nili Fossae and implications for aqueous alteration, *J. Geophys. Res.*, *114*, E00D08, doi:10.1029/2009JE003339.

Elwood Madden, M. E., R. J. Bodnar, and J. D. Rimstidt (2004), Jarosite as an indicator of water-limited chemical weathering on Mars, *Nature*, *431*, 821–823, doi:10.1038/nature02971.

Elwood Madden, M. E., A. S. Madden, and J. D. Rimstidt (2009), How long was Meridiani Planum wet?: Applying a jarosite stopwatch to determine the duration of aqueous diagenesis, *Geology*, *37*, 635–638, doi:10.1130/G25639A.1.

Fairén, A. G., D. Schulze-Makuch, A. P. Rodríguez, W. Fink, A. F. Davila, E. R. Uceda, R. Furfaro, R. Amils, and C. P. McKay (2009), Evidence for Amazonian acidic liquid water on Mars: A reinterpretation of MER mission results, *Planet. Space Sci.*, *57*, 276–287, doi:10.1016/j.pss.2008.11.008.

Farrand, W. H., T. D. Glotch, J. W. Rice Jr., J. A. Hurowitz, and G. A. Swayze (2009), Discovery of jarosite within the Mawrth Vallis region of Mars: Implications for the geologic history of the region, *Icarus*, *204*, 478–488, doi:10.1016/j.icarus.2009.07.014.

Fernández-Remolar, D. C., R. V. Morris, J. E. Gruener, R. Amils, and A. H. Knoll (2005), The Río Tinto Basin, Spain: Mineralogy, sedimentary geobiology, and implications for interpretation of outcrop rocks at Meridiani Planum, Mars, *Earth Planet. Sci. Lett.*, *240*, 149–167, doi:10.1016/j.epsl.2005.09.043.

Gray, D. J. (2001), Hydrogeochemistry in the Yilgarn Craton, *Geochem. Explor. Environ. Anal.*, *1*, 253–264.

Hay, R. L. (1964), Phillipsite of saline lakes and soils, *Am. Mineral.*, *49*, 1366–1387.

Hay, R. L. (1973), Lithofacies and environments of Bed I, Olduvai Gorge, Tanzania, *Quat. Res.*, *3*, 541–560, doi:10.1016/0033-5894(73)90030-6.

Hay, R. L. (1976), *Geology of the Olduvai Gorge: A Study of Sedimentation in a Semiarid Basin*, Univ. of Calif. Press, Berkeley.

Hay, R. L., and T. K. Kyser (2001), Chemical sedimentology and paleoenvironmental history of Lake Olduvai, a Pliocene lake in northern Tanzania, *Geol. Soc. Am. Bull.*, *113*, 1505–1521, doi:10.1130/0016-7606(2001)113<1505:CSAPHO>2.0.CO;2.

Hover, V. C., and G. M. Ashley (2003), Geochemical signatures of paleodepositional and diagenetic environments: A STEM/AEM study of authigenic clay minerals from an arid rift basin, Olduvai Gorge, Tanzania, *Clays Clay Minerals*, *51*, 231–251, doi:10.1346/CCMN.2003.0510301.

Klingelhöfer, G., et al. (2003), Athena MIMOS II Mössbauer spectrometer investigation, *J. Geophys. Res.*, *108*(E12), 8067, doi:10.1029/2003JE002138.

Klingelhöfer, G., et al. (2004), Jarosite and hematite at Meridiani Planum from Opportunity's Mössbauer spectrometer, *Science*, *306*, 1740–1745, doi:10.1126/science.1104653.

Knoll, A. H., et al. (2005), An astrobiological perspective on Meridiani Planum, *Earth Planet. Sci. Lett.*, *240*, 179–189, doi:10.1016/j.epsl.2005.09.045.

Langella, A., P. Cappelletti, and M. de'Gennaro (2001), Zeolites in closed hydrologic systems, in *Sulfate Minerals: Crystallography, Geochemistry, and Environmental Significance*, edited by C. N. Alpers, J. L. Jambor, and D. K. Nordstrom, pp. 235–260, Mineral. Soc. of Am., Washington, D. C.

Leclerc, A. (1980), Room temperature Mössbauer analysis of jarosite-type compounds, *Phys. Chem. Minerals*, *6*, 327–334, doi:10.1007/BF00307622.

Leveille, R. J. (2007), Formation of jarosite and Mars-like minerals in a polar desert: Implications for Mars aqueous geochemistry, *Geol. Soc. Am. Abstr. Programs*, *39*(6), 284.

McHenry, L. J. (2005), Phenocryst composition as a tool for correlating fresh and altered tephra, Bed I, Olduvai Gorge, Tanzania, *Stratigraphy*, *2*, 101–115.

McHenry, L. J. (2009), Element mobility during zeolitic and argillic alteration of volcanic ash in a closed-basin lacustrine environment: Case study Olduvai Gorge, Tanzania, *Chem. Geol.*, *265*, 540–552, doi:10.1016/j.chemgeo.2009.05.019.

McHenry, L. J. (2010), Element distribution between coexisting authigenic mineral phases in argillic and zeolitic altered tephra, Olduvai Gorge, Tanzania, *Clays Clay Minerals*, *58*(5), 627–643, doi:10.1346/CCMN.2010.0580504.

McHenry, L. J. (2011), A revised stratigraphic framework for Olduvai Gorge Bed I based on tuff geochemistry, *J. Hum. Evol.*, in press.

McHenry, L. J., G. M. Mollel, and C. C. Swisher III (2008), Compositional and textural correlations between Olduvai Gorge Bed I tephra and volcanic sources in the Ngorongoro Volcanic Highlands, Tanzania, *Quat. Int.*, *178*, 306–319, doi:10.1016/j.quaint.2007.01.004.

McSween, H. Y., et al. (2006), Characterization and petrologic interpretation of olivine-rich basalts at Gusev Crater, Mars, *J. Geophys. Res.*, *111*, E02S10, doi:10.1029/2005JE002477.

McSween, H. Y., G. J. Taylor, and M. B. Wyatt (2009), Elemental composition of the Martian crust, *Science*, *324*, 736–739, doi:10.1126/science.1165871.

Milliken, R. E., et al. (2008), Opaline silica in young deposits on Mars, *Geology*, *36*, 847–850, doi:10.1130/G24967A.1.

Ming, D. W., et al. (2006), Geochemical and mineralogical indicators for aqueous processes in the Columbia Hills of Gusev crater, Mars, *J. Geophys. Res.*, *111*, E02S12, doi:10.1029/2005JE002560.

Morris, R. V., D. W. Ming, D. C. Golden, and J. F. Bell III (1996), An occurrence of jarositic tephra on Mauna Kea, Hawaii: Implications for the ferric mineralogy of the Martian surface, in *Mineral Spectroscopy: A Tribute to Roger G. Burns*, *Spec. Publ. Geochem Soc.*, 5, edited by M. D. Dyar, C. McCammon, and M. W. Schaefer, pp. 327–336, Geochem. Soc., St. Louis, Mo.

Morris, R. V., et al. (2006a), Mössbauer mineralogy of rock, soil, and dust at Gusev crater, Mars: Spirit's journey through weakly altered olivine basalt on the plains and pervasively altered basalt in the Columbia Hills, *J. Geophys. Res.*, *111*, E02S13, doi:10.1029/2005JE002584.

Morris, R. V., et al. (2006b), Mössbauer mineralogy of rock, soil, and dust at Meridiani Planum, Mars: Opportunity's journey across sulfate-rich outcrop, basaltic sand and dust, and hematite lag deposits, *J. Geophys. Res.*, *111*, E12S15, doi:10.1029/2006JE002791.

Murchie, S., et al. (2009), Evidence for the origin of layered deposits in Candor Chasma, Mars, from mineral composition and hydrologic modeling, *J. Geophys. Res.*, *114*, E00D05, doi:10.1029/2009JE003343 [printed 115(E2), 2010].

Niles, P. B., and J. R. Michalski (2009), Meridiani Planum sediments on Mars formed through weathering in massive ice deposits, *Nat. Geosci.*, *2*, 215–220, doi:10.1038/ngeo438.

Papike, J. J., J. M. Karner, and C. K. Shearer (2006), Comparative planetary mineralogy: Implications of Martian and terrestrial jarosite: A crystal chemical perspective, *Geochim. Cosmochim. Acta*, *70*, 1309–1321, doi:10.1016/j.gca.2005.11.004.

Poulet, F., R. E. Arvidson, C. Gomez, R. V. Morris, J.-P. Bibring, Y. Langevin, B. Gondet, and J. Griffes (2008), Mineralogy of Terra Meridiani and western Arabia Terra from OMEGA/MEx and implications for their formation, *Icarus*, *195*, 106–130, doi:10.1016/j.icarus.2007.11.031.

Reid, D. A., R. C. Graham, S. B. Edinger, L. H. Bowen, and J. O. Ervin (1988), Celadonite and its transformation to smectite in an entisol at Red Rock Canyon, Kern County, California, *Clays Clay Minerals*, *36*, 425–431, doi:10.1346/CCMN.1988.0360507.

Rieder, R., et al. (2004), Chemistry of rocks and soils at Meridiani Planum from the Alpha Particle X-ray Spectrometer, *Science*, *306*, 1746–1749, doi:10.1126/science.1104358.

Roach, L. H., J. F. Mustard, G. Swayze, R. E. Milliken, J. L. Bishop, S. L. Murchie, and K. Lichtenberg (2010), Hydrated mineral stratigraphy of Ius Chasma, Valles Marineris, *Icarus*, *206*, 253–268, doi:10.1016/j.icarus.2009.09.003.

Ruff, S. W. (2004), Spectral evidence for zeolite in the dust on Mars, *Icarus*, *168*, 131–143, doi:10.1016/j.icarus.2003.11.003.

Stoffregen, R. E., C. N. Alpers, and J. L. Jambor (2000), Alunite-jarosite crystallography, thermodynamics, and geochemistry, in *Sulfate Minerals: Crystallography, Geochemistry, and Environmental Significance*, edited by C. N. Alpers, J. L. Jambor, and D. K. Nordstrom, pp. 453–480, Mineral. Soc. of Am., Washington, D. C.

Stollhofen, H., I. G. Stanistreet, L. J. McHenry, G. F. Mollel, R. J. Blumenschine, and F. T. Masao (2008), Fingerprinting facies of the Tuff IF marker, with implications for early hominin palaeoecology, Olduvai

Gorge, Tanzania, *Palaeogeogr. Palaeoclimatol. Palaeoecol.*, *259*, 382–409, doi:10.1016/j.palaeo.2007.09.024.

Tosca, N. J., S. M. McLennan, B. C. Clark, J. P. Grotzinger, J. A. Hurowitz, A. H. Knoll, C. Schröder, and S. W. Squyres (2005), Geochemical modeling of evaporation processes on Mars: Insight from the sedimentary record at Meridiani Planum, *Earth Planet. Sci. Lett.*, *240*, 122–148, doi:10.1016/j.epsl.2005.09.042.

Tosca, N. J., S. M. McLennan, M. D. Dyar, E. C. Sklute, and F. M. Michel (2008), Fe oxidation processes at Meridiani Planum and implications for secondary Fe mineralogy on Mars, *J. Geophys. Res.*, *113*, E05005, doi:10.1029/2007JE003019.

Tuttle, M. L. W., and G. N. Breit (2009), Weathering of the New Albany Shale, Kentucky, USA: I. Weathering zones defined by mineralogy and major-element composition, *Appl. Geochem.*, *24*, 1549–1564, doi:10.1016/j.apgeochem.2009.04.021.

Walter, R. C., P. C. Manega, and R. L. Hay (1992), Tephrochronology of Bed I, Olduvai Gorge: An application of laser-fusion $^{40}Ar/^{39}Ar$ dating to calibrating biological and climatic change, *Quat. Int.*, *13–14*, 37–46, doi:10.1016/1040-6182(92)90008-P.

Wray, J. J., S. L. Murchie, S. W. Squyres, F. P. Seelos, and L. L. Tornabene (2009), Diverse aqueous environments on ancient Mars revealed in the southern highlands, *Geology*, *37*, 1043–1046, doi:10.1130/G30331A.1.

Wray, R., E. Milliken, G. A. Swayze, C. M. Dundas, J. L. Bishop, S. L. Murchie, F. P. Seelos, and S. W. Squyres (2009), Columbus Crater and other possible paleolakes in Terra Sirenum, Mars, *Lunar Planet. Sci.*, *XLI*, Abstract 1896.

V. Chevrier, W. M. Keck Laboratory for Space and Planetary Simulation, Arkansas Center for Space and Planetary Sciences, MUSE 202, University of Arkansas, Fayetteville, AR 72701, USA. (vchevrie@uark.edu)

L. J. McHenry, Department of Geosciences, University of Wisconsin-Milwaukee, 3209 N. Maryland Ave., Milwaukee, WI 53211, USA. (lmchenry@uwm.edu)

C. Schröder, Center for Applied Geoscience, Eberhard Karls Universität, Sigwartstr. 10, D-72076 Tübingen, Germany. (christian.schroeder@ifg.uni-tuebingen.de)